Available online at www.sciencedirect.com

SCIENCE DIRECT®

Bioelectrochemistry 67 (2005) 91 – 99

Bioelectrochemistry

www.elsevier.com/locate/bioelechem

Excluded volume driven counterion condensation inside nanotubes in a concave electrical double layer model

Klemen Bohinc[a,b], Jan Gimsa[c], Veronika Kralj-Iglič[d], Tomaž Slivnik[a], Aleš Iglič[a,*]

[a]*Laboratory of Physics, Faculty of Electrical Engineering, Tržaška 25, SI-1000 Ljubljana, Slovenia*
[b]*University College of Health Care, University of Ljubljana, Poljanska 26a, 1000 Ljubljana, Slovenia*
[c]*University of Rostock, Department of Biology, Gertrudenstr. 11 A, D-18051 Rostock, Germany*
[d]*Institute of Biophysics, Medical Faculty, Lipičeva 2, SI-1000 Ljubljana, Slovenia*

Received 3 September 2004; received in revised form 31 December 2004; accepted 7 January 2005
Available online 10 May 2005

Abstract

The physical properties of organic nanotubes attract increasing attention due to their potential benefit in technology, biology and medicine. We study the effect of ion size on the electrical properties of cylindrical nanotubes filled with electrolyte solution within a modified Poisson–Boltzmann (PB) approach. For comparison purposes, small hollow nanospheres filled with electrolyte solution are considered. The finite size of the particles in the inner electrolyte solution is described by the excluded volume effect within a lattice statistics approach. We found that an increased ion size reduces the number of counterions near the charged inner surface of the nanotube, leading to an enlarged electrostatic surface potential. The concentration of counterions close to the inner surface saturates for higher surface charge densities and larger ions. In the case of saturation, the closest counterion packing is achieved, all lattice sites near the surface are occupied and an actual counterion condensation is observed. By contrast, the counterion concentration at the axis of the nanotube steadily increases with increasing surface charge density. This growth is more pronounced for smaller nanotube radii and larger ions. At larger nanotube radii for small ion size counterion condensation may also be observed according to the Tsao criterion, i.e. the counterion concentration at the centre is independent of the number of counterions in the system. With decreasing radius the Tsao condensation effect is shifted towards physiologically unrealistic surface charge densities.
© 2005 Elsevier B.V. All rights reserved.

Keywords: Nanotubes; Reverse osmosis; Excluded volume effect; Lattice statistics

1. Introduction

Recently, much attention is being devoted to inorganic and organic hollow cylindrical structures in the nanometer range due to their potential benefit in technology, biology and medicine [1]. Potential applications range from microelectronics to microfluidics [2]. Among other systems, nanotubes have been found in different phospholipid systems [2,3]. In cellular systems a direct transport between different cells or cellular organelles has been observed through hollow nanotubes or by carrier vesicles guided by nanotubes [4]. Ion channels or pores in biological membranes and blood capillaries are also examples for cylindrical nanotubes.

In some biological systems, the walls of organic nanotubes are charged and in contact with electrolyte solution. Due to the surface charge of the walls, counterions and coions of the electrolyte are, respectively, accumulated and depleted near the walls. At the internal surfaces concave electrical double layers of cylindrical geometry are formed [5,6].

Concave electrical double layers may also be of spherical shape, like in cavities which may be filled with aqueous electrolytes. Examples from biology and colloid chemistry are self-assembling dispersions such as spherical inverse micelles, phospholipid vesicles and microemulsions [5,7]. Such objects are formed by aggregation of amphiphilic molecules in a way that the hydrophilic

* Corresponding author. Tel.: +386 1 4768 235; fax: +386 1 4268 850.
E-mail address: klemen.bohinc@fe.uni-lj.si (K. Bohinc).

1567-5394/$ - see front matter © 2005 Elsevier B.V. All rights reserved.
doi:10.1016/j.bioelechem.2005.01.004

parts of the molecules are in contact with electrolyte solutions, while the hydrophobic parts avoid such contact. While micelles are small aggregates of amphiphilic molecules in aqueous solutions, microemulsions are formed in mixtures of amphiphiles, water and oil, where domains of water (in oil) or oil (in water) are separated by surfactant monolayers. Multilamellar vesicles can then be formed by a number of surfactant bilayers separating an internal compartment from the continuous phase of a solution.

In thin nanotubes and small spherical vesicles, the granularity of the constituting molecules, ions or atoms approaches the smallest extension of the entire structure. Therefore, the validity of the standard continuum approach cannot be taken for granted, even for a qualitative description of these systems [3,1]. A correct description of the aqueous double layers should take the finite size of the ions and water molecules into account, especially on their inner surfaces [8–11]. A possible approach to the improvement requires an extension of the classical continuum treatment based on the PB theory treating ions as charged points [12–15].

A number of different attempts have been made to incorporate steric effects into the PB equation. Freise [16] introduced the excluded volume effect by a pressure-dependent potential, while Eigen and Wicke [17] used a thermodynamic approach, multiplying the numerical density of ions by a factor containing the number of the vacant sites. More recently, the finite size of particles has been incorporated into the PB theory in more transparent ways, based on a lattice statistics model [8–11], functional approaches [18–20] or on a model that takes the surface charge correlation into account, while treating ions and solvent molecules as hard spheres [21]. In addition to the finite size of particles, the fluctuation potential has been introduced [22]. These approaches lead to a better agreement with Monte Carlo (MC) simulations for divalent counterions [23]. For such ions, an even better agreement of the MC simulations was found, also for divalent ions, when the hypernetted chain integral equations were applied [24,25].

This work aims to describe the effect of ion size on the properties of the electrical double layer within cylindrical nanotubes. Double layers within hollow spheres are considered for comparison purposes. We use a modified form of the PB theory that has been obtained from the PB theory by introducing the excluded volume effect in order to describe the counterion distribution and the electrostatic potential near the charged surface. This is accordingly designated EVPB theory in the text.

In addition, the counterion condensation will be examined. Expressions for the free energy, the ion distribution function and the differential equation for the electrostatic potential will be derived in the Appendix. All results will be compared to the classical PB theory.

2. Theory

Charged cylindrical or spherical surfaces may create concave electrical double layers when in contact with an electrolyte solution. The surfaces are assumed to carry the surface charge density σ. The electrolyte solutions should be composed of solvent molecules and M species of ions. The geometry of cylindrical surfaces is described by radius r_0 and length l, while spherical surfaces are described by r_0 (Figs. 1, 2). For reasons of symmetry, the electric field must vanish at the cylinder axis or in the centre of the sphere.

The electrostatic interactions are described within the mean field approximation while the finite size of the particles in the solution is considered by means of the excluded volume effect. The latter is taken into account by a statistical mechanics description, where each particle in the solution occupies one and only one site of a finite volume. A lattice with an adjustable lattice constant has been introduced [26]. All sites of the lattice are filled with solvent molecules or ions. The density of the number of lattice sites of the system n_s is given by

$$n_s = \sum_{j=0}^{M} n_j(r), \tag{1}$$

where n_0 is the density of the number of solvent molecules, n_j are the densities of the number of ions of the j-th species, with $j=1, 2, \ldots, M$, and r is the radial coordinate, respectively. n_s can be calculated from the volume of a three-dimensional lattice site V_s, $n_s=1/V_s$. The lattice sites are taken to have equal volumes V_s, which could be calculated from the lattice constant $V_s=a^3$. Thus,

$$n_s = \frac{1}{a^3}. \tag{2}$$

Different values of the lattice constant a describe different sizes of the ions. In the following the density of

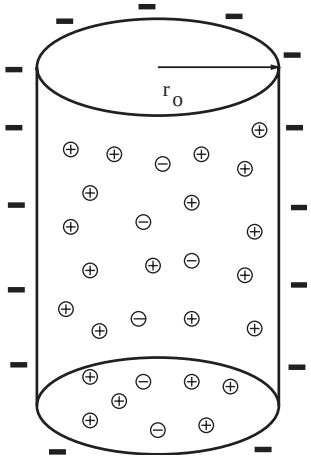

Fig. 1. Schematic presentation of a cylindrical electrical double layer of concave shape, σ is negative. The cations are accumulated near the charged surface while the anions are depleted from this region.

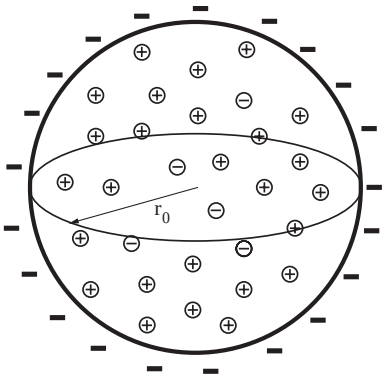

Fig. 2. Schematic presentation of a spherical electrical double layer of concave shape, σ is negative. The cations are accumulated near the spherical surface while the anions are depleted from this region.

the number of counterions is referred to as concentration. Changes in the counterion size have been simulated by choosing an appropriate a.

The electrostatic field and the ion concentrations are defined for all values of radial coordinates. For both geometries of the charged surface, the mean electrostatic potential $\Phi(r)$ can be calculated from the EVPB theory (see Appendix):

$$\frac{\mathrm{d}^2\Phi(r)}{\mathrm{d}r^2}+\frac{\eta}{r}\frac{\mathrm{d}\Phi(r)}{\mathrm{d}r} = -\frac{e_0 n_s\left(\sum_{i=1}^{M} v_i(n_{ic}/n_{0c})\exp(-v_i e_0(\Phi(r)-\Phi_c)/kT)\right)}{\epsilon\epsilon_0\left(1+\sum_{i=1}^{M}(n_{ic}/n_{0c})\exp(-v_i e_0(\Phi(r)-\Phi_c)/kT)\right)}, \tag{3}$$

where e_0 is the elementary charge, v_i is the valency of the ions of the i-th species, n_{ic} denotes the concentration of particles of the i-th species at $r=0$; Φ_c denotes the electrostatic potential at the cylinder axis or in the centre of the sphere, ϵ is the relative dielectric constant of the solution, ϵ_0 is the permittivity of vacuum, T is the temperature and k is the Boltzmann constant. The constant η depends on the geometry of the system. In spherical geometry $\eta=2$ while in cylindrical geometry $\eta=1$.

The particle distribution functions are

$$n_j(r)=\frac{n_s(n_{jc}/n_{0c})\exp(-v_j e_0(\Phi(r)-\Phi_c)/kT)}{1+\sum_{i=1}^{M}(n_{ic}/n_{0c})\exp(-v_i e_0(\Phi(r)-\Phi_c)/kT)} \quad j=0,1,2,\ldots,M. \tag{4}$$

The Eqs. (3) and (4) are the result of the minimisation procedure given in the Appendix.

In order to obtain the explicit dependence of n_j and Φ on distance r, the differential Eq. (3) was solved numerically. The first boundary condition states that the electrical field is zero at the axis of cylinder and in the centre of sphere:

$$\left.\frac{\mathrm{d}\Phi(r)}{\mathrm{d}r}\right|_{r=0}=0. \tag{5}$$

The second boundary condition in the vicinity of the charged surface of concave shape demands a neutral overall charge for the system:

$$\left.\frac{\mathrm{d}\Phi(r)}{\mathrm{d}r}\right|_{r=r_0}=-\frac{\sigma}{\epsilon\epsilon_0}. \tag{6}$$

By integration of Eq. (3) we obtain:

$$\int_0^{r_0}\sum_{j=1}^{M} e_0 v_j n_j(r) J(r)\mathrm{d}r+\sigma S_0=0, \tag{7}$$

where in the spherical geometry $J(r)=4\pi r^2$ and $S_0=4\pi r_0^2$ while in the cylindrical geometry $J(r)=2\pi rl$ and $S_0=2\pi r_0 l$. The first and second terms in Eq. (7) represent the charges of the solution and the surface, respectively.

For numerical calculations, the fourth-order Runge–Kutta method was combined with the shooting method and applied to Eq. (3). For solving the equation calculations were started at the axis of the cylinder or in the centre of the sphere. The concentration of counterions was varied to satisfy the boundary condition (6) for every given potential Φ_c and concentration of coions at the axis of the cylinder or in the centre of the sphere n_{co}^c.

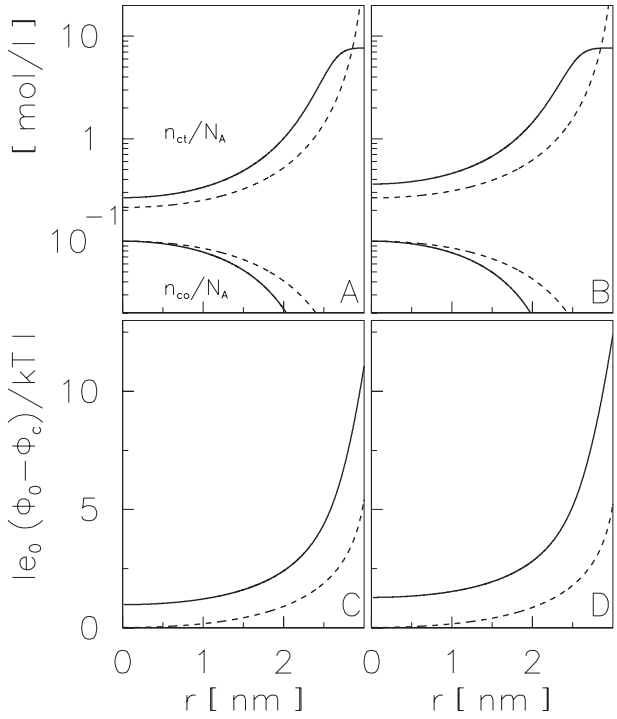

Fig. 3. $n_{ct}(r)$ and $n_{co}(r)$ for cylindrical (A) and spherical (B) concave geometries. Electrostatic potential $|e_0(\Phi_0-\Phi_c)/kT|$ for cylindrical (C) and spherical (D) concave geometries in dependence on the radial distance (r). The results of the EVPB theory with $a=0.6$ nm (solid lines) and the results of the PB theory (dashed lines) are shown. The model parameters are $\epsilon=78.5$, $T=296$ K, $n_{co}^c=0.1$ mol/l, $r_0=3$ nm and $\sigma=0.4$ As/m^2.

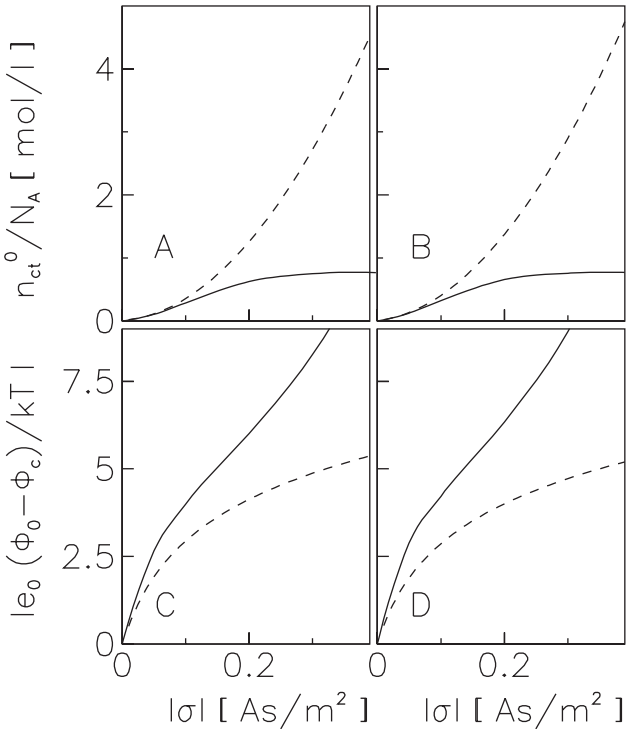

Fig. 4. n_{ct}^0 at the distance of closest approach to the charged cylindrical (A) and spherical (B) concave surfaces. Electrostatic potential $|e_0(\Phi_0-\Phi_c)/kT|$ at the distance of closest approach to the charged cylindrical (C) and spherical (D) concave surfaces as a function of $|\sigma|$. Results of the PB theory are given by dashed lines, whereas the calculations for $a=0.6$ nm are given by solid lines. Model parameters are $\epsilon=78.5$, $T=296$ K, $r_0=3$ nm and $n_{co}^c=0.1$ mol/l.

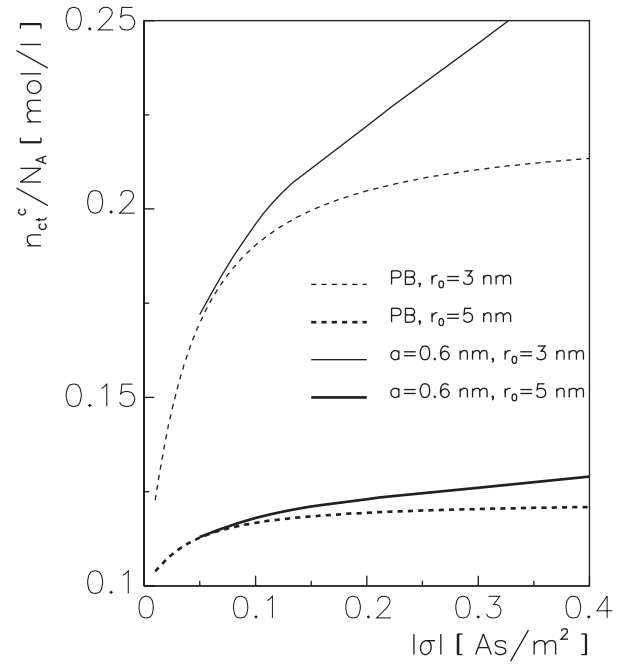

Fig. 5. Cylindrical electrical double layer of concave shape. n_{ct}^c as a function $|\sigma|$ for two different radii of the cylinder $r_0=3$ nm (thin lines) and $r_0=5$ nm (bold lines) are presented. The results of the PB theory are shown by dashed lines, whereas the calculations for $a=0.6$ nm are shown by solid lines. The model parameters are $\epsilon=78.5$, $T=296$ K and $n_{co}^c=0.1$ mol/l.

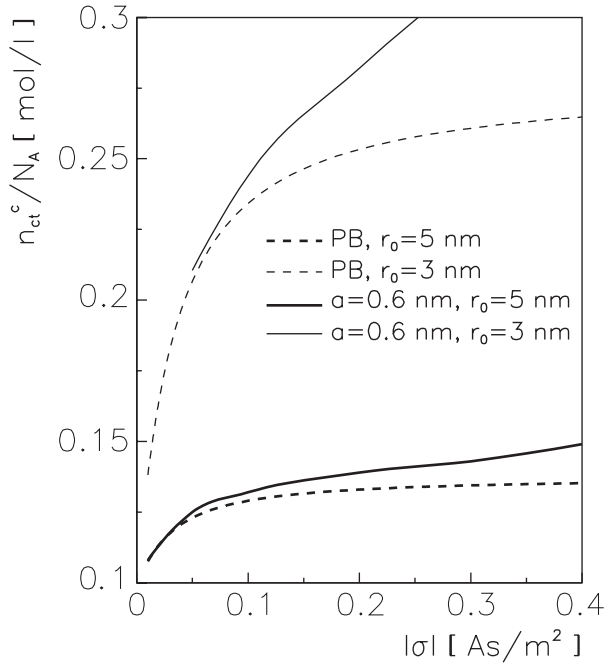

Fig. 6. Spherical electrical double layer of concave shape. n_{ct}^c as a function of $|\sigma|$ for two different radii of the sphere $r_0=3$ nm (thin lines) and $r_0=5$ nm (bold lines) are presented. The results of the PB theory are shown by dashed lines, whereas the calculations for $a=0.6$ nm are shown by solid lines. The model parameters are $\epsilon=78.5$, $T=296$ K and $n_{co}^c=0.1$ mol/l.

3. Results

Fig. 3 presents the concentration profiles of the counterion (M_{ct}) and coion (M_{co}) concentrations as well as the potential profiles for cylindrical and spherical double layers. The figure also compares our EVPB results to the

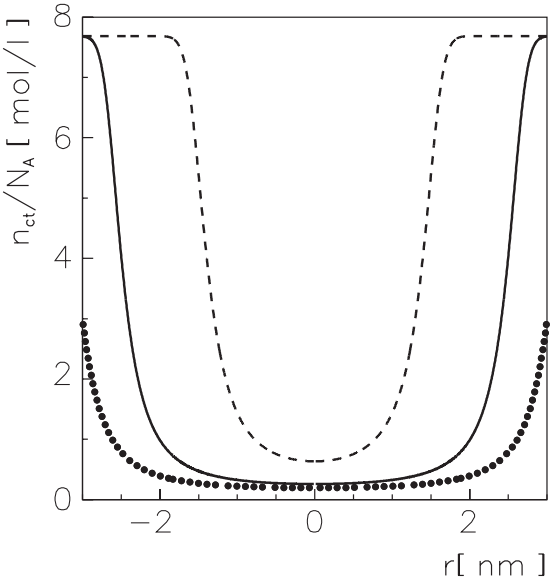

Fig. 7. The profile $n_{ct}(r)$ for cylindrical concave geometry. The results of the EVPB theory with $a=0.6$ nm for $\sigma=0.7$ As/m^2 (dashed line), $\sigma=0.4$ As/m^2 (solid line) and $\sigma=0.1$ As/m^2 (dotted line) are shown. The model parameters are $\epsilon=78.5$, $T=296$ K and $n_{co}^c=0.1$ mol/l, and $r_0=3$ nm.

predictions of the classical PB theory for a symmetric univalent electrolyte ($\nu_{ct}=1$ and $\nu_{co}=-1$). The theoretical predictions of the PB and EVPB theories differ significantly for both geometries in the vicinity of the surfaces while they come closer at the cylinder axis or the centre of the sphere. In EVPB theory, the profile of counterion concentration exhibits a plateau region near the surface for sufficiently large a values, whereas for vanishing a the concentration of counterions converges towards the value obtained by the PB theory. Note that the concentration of coions at the cylinder axis or in the centre of the sphere is always smaller than the corresponding counterion concentration. This is a consequence of the electroneutrality condition. In the model used the charge overcompensation is not obtained [26].

Fig. 4A and B show the counterion concentration at the surface in dependence on the absolute value of the σ ($|\sigma|$). Fig. 4C and D show $|\Phi_0-\Phi_c|$ as a function of $|\sigma|$, where Φ_0 is the electrostatic potential at the charged surface and Φ_c is the electrostatic potential at the axis of the cylinder and in the centre of the sphere, respectively. The discrepancy between classical PB and EVPB theories intensifies with increasing $|\sigma|$. In PB theory, the concentration of counterions close to the charged surface n_{ct}^0 continuously increases as a function of $|\sigma|$ at high surface charge densities too, while it reaches a plateau in the EVPB theory (Fig. 4A and B). For small $|\sigma|$, the values of the electrostatic potential near the surface coincide for both theories, while the discrepancy increases with increasing $|\sigma|$.

Figs. 5 and 6 show the concentration of counterions at the axis of the cylinder (M_{ct}^c) and in the centre of the sphere (M_{ct}^c) in dependence on $|\sigma|$ for two different radii of cylindrical and spherical surfaces. In PB theory, the counterion concentration at the axis of the cylinder or in the centre of the sphere may saturate at an upper limit for high surface charge densities [27,28] (dashed lines in Figs. 5 and 6). This feature is specific to concave surfaces confining an electrolyte solution in PB theory. Nevertheless, saturation can only be observed for larger radii of the concave surface. Interestingly, no saturation of counterion concentration in the centre has been observed in the EVPB theory.

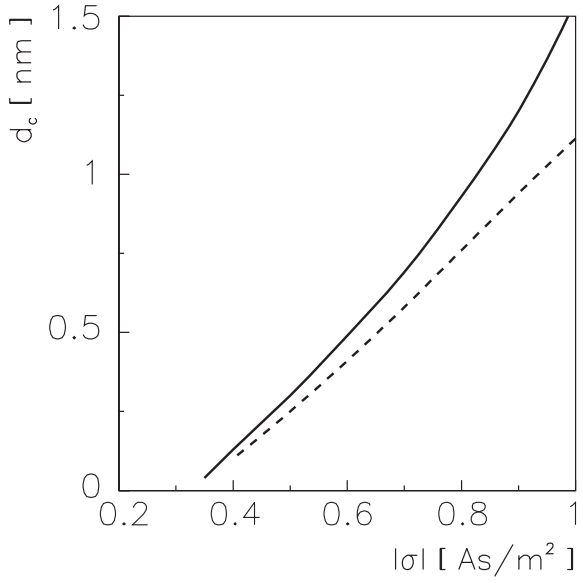

Fig. 8. d_c as a function of $|\sigma|$ for two different radii of the cylinder $r_0=3$ nm (solid line) and $r_0=5$ nm (dashed line). The EVPB theory was used. The model parameters are $\epsilon=78.5$, $T=296$ K and $n_{co}^c=0.1$ mol/l.

Fig. 7 shows the counterion concentration profiles for cylindrical electrical double layers for three different values of a. The EVPB theory was applied to a symmetric univalent electrolyte ($\nu_{ct}=1$ and $\nu_{co}=-1$). For ions of sufficient size ($a=0.6$ nm) and $|\sigma|$ a plateau region near the charged surface occurs. The plateau region increases with $|\sigma|$. At small $|\sigma|$ no plateau is observed. Fig. 8 shows the thickness of the plateau region d_c as a function of $|\sigma|$ for two different radii of the cylinder. d_c increases with increasing $|\sigma|$, the increase is more pronounced for smaller radii of the cylinder. The thickness d_c has been defined as the extension of the plateau, where the counterion concentration drops to 99% of its surface value.

4. Discussion and conclusion

The introduction of the excluded volume effect in the PB theory through the lattice model approach allows for an improved description of the electrostatics of charged cylindrical nanotubes and nanospheres filled with electrolyte solution. Even though the ion size is described by a lattice constant, the ion concentration is defined at any distance to the surface. Therefore continuous functions can be derived for the particle distribution and the electrostatic potential. The model distinguishes between occupied and free lattice sites. Free lattice sites are assumed to be occupied by water with a relative permittivity of 78.5. Consequently, the ions are assumed to be suspended in a continuous dielectric medium.

In PB theory, ions are considered to be dimensionless. Thus, the counterion concentration near a charged surface can increase boundlessly (compare to Fig. 3A,B). As a result, the results of the PB theory show a continuous increase in counterion concentration near the surface, with increasing $|\sigma|$ (Fig. 4). In contrast to the PB theory, in EVPB theory ions are assumed to have a finite size. This assumption has a considerable effect on counterion concentration and the electrostatic potential profiles. The EVPB theory predicts a plateau of counterion concentration close to the concave surface [9], a finding supported by recent experimental findings on planar electrical double layers [29]. The deviation from the predictions of the PB theory must be attributed to the steric effect (Figs. 3 and 4) where the number density of ions cannot exceed the density of the lattice sites.

In PB theory a change in the behavior of the counterion concentration profile in the vicinity of the surface, i.e. counterion condensation, may be observed with increasing

$|\sigma|$. An indirect criterion for counterion condensation within the PB for concave double layers was recently introduced by Tsao [27,28]. Tsao stated that for sufficiently large $|\sigma|$ the concentrations of counterions in the vicinity of the geometrical axis of a cylinder or in the centre of a sphere are not affected by growing $|\sigma|$. This behavior is analog to an equithermal system of vapor and water where added evaporated water would undergo a phase transition increasing the volume of the condensed water phase. The condensed and the gaseous water phases are at equilibrium and the vapor pressure is constant at a given temperature.

The prediction of the PB theory may be well understood since at large $|\sigma|$, counterions are depleted from the central regions due to the strong attraction by the charged surface, leading to a constant counterion concentration in the central regions of the solution (Fig. 5).

Nevertheless, one prerequisite for the observability of this effect is a larger radius r_0 in order to avoid overlapping double layers of the opposite surfaces. An analogous explanation applies to concave spherical double layers (Fig. 6). Within the physiological range for $|\sigma| \leq 0.4$ As/m^2 counterion condensation according to Tsao's criterion occurs only for radii larger than $r_0=5$ nm as can be seen in Figs. 5 and 6. It starts at around $|\sigma| \approx 0.2$ As/m^2.

In both the PB and EVPB theories, the fulfillment of the Tsao criterion for counterion condensation depends on the radius of the sphere and the cylinder. According to the Tsao criterion, with decreasing radius, the condensation is less pronounced at physiological $|\sigma|$ values, due to an overlap of the double layers of the opposite surfaces (Fig. 7). Whereas (according to the Tsao criterion) condensation may be shifted towards higher $|\sigma|$ values in PB theory, it vanishes in accordance with EVPB theory. This can be seen in Figs. 5 and 6 (solid curves) where the EVPB theory predicts a monotonous increase in n_{ct}^{c} with $|\sigma|$. This increase is more pronounced for smaller nanotube radii (r_0) and larger ion radii due to a relative or absolute increase in the electrical double layer thickness (Fig. 7). In the limit of very large radii of the nanotubes, when the system approaches two planar surfaces, the EVPB theory also predicts a constant counterion concentration in the central region, consistent with Tsao's criterion.

For large $|\sigma|$ and a the EVPB theory predicts that all lattice sites are occupied by counterions leading to a plateau in the counterion concentration profile close to the surface. In the limiting case of very large nanotube radii, d_c linearly increases with $|\sigma|$ (Fig. 8, dashed line). This behavior is in keeping with the dense packing (condensation) model for planar charged surface, $d_c = \frac{|\sigma| a^3}{e_0}$. For smaller nanotube radii, geometry limits the available lattice sites, leading to a growth in d_c with $|\sigma|$ which is stronger than in the linear regime for larger radii. At $|\sigma|$ where $d_c=a$ the first counterion layer is completely occupied, representing a single Helmholtz layer of thickness a with linear electrostatic potential profile. The condition to be met for the first layer is:

$$\frac{1}{A}\int_0^a n_{ct} \mathrm{d}V = \frac{1}{a^2} \tag{8}$$

which is equivalent to the condition $d_c=a$ (Fig. 8). It can be seen (Fig. 8) that the first layer of the nanotubes of radius $r_0=3$ nm is completely occupied for $|\sigma| \approx 0.65$ As/m^2, while the second layer for $|\sigma| \approx 0.9$ As/m^2.

Accordingly, two different counterion phases may exist in the EVPB model, a condensed one of thickness $d_c=a$, $d_c=2a,..$ near the charged surface and the electrolyte solution with freely moving counterions, coions, and water. Condensation represents a phase transition for the counterions from a state where they are subject to the interplay of electric and entropic forces to a state where the electrostatic interaction defeats the entropic interactions arranging them in a closely packed structure. The thickness of the condensed layer d_c increases with $|\sigma|$ and ion size (Fig. 8). The phase properties of the condensed counterions are largely independent of system parameter changes, e.g. a further increase in $|\sigma|$. The close packing of counterions near the charged surface can be considered an actual condensation inherent to the EVPB theory.

With decreasing radius, the number of lattice sites declines faster in the spherical than in the cylindrical geometry. Therefore the concentration of counterions at the axis of a cylinder reaches a plateau at lower $|\sigma|$ than in the centre of a sphere. In cylindrical geometry, counterion condensation is observed at lower $|\sigma|$ than in spherical geometry.

Nanotubes of erythrocyte membrane were obtained by the membrane budding induced by adding certain detergents to the erythrocyte suspension [30]. As the inner side of the erythrocyte membrane contains phosphatidylserine molecules that are at physiological pH values negatively charged the observed nanotubes would represent a system that could be subject to the theory considered in this work. Membranes with narrow capillaries possessing highly charged walls are employed in reverse osmosis [31]. The physico–chemical properties of the capillaries are mainly determined by their electrical double layer properties. In particular, the electrical double layer thickness, particle and ion size influence the flow of a solution through the capillaries. It seems very likely that in EVPB theory the relationships inside the pores, especially the excluded volume effect, are described in a more realistic way than in most other theories. Nevertheless, a thorough investigation of the consequences of this model in order to achieve a better understanding of the process of reverse osmosis is beyond the scope of this manuscript.

The EVPB theory makes it possible to study the physical properties of hollow nanotubes at high surface charge densities, confining large ions to the inner electrolyte solutions. In contrast, the PB theory is limited to $|\sigma|$ values below $|\sigma| \approx 0.15$ As/m^2, where the number density of counterions exceeds the number density of lattice sites

(Fig. 4). EVPB theory can easily be extended to more complicated nanosystems and geometries.

One restriction in the presented EVPB approach is that ion–ion interactions other than the hard core interaction are neglected. Nevertheless, in the case of monovalent ions, the ion–ion interaction effects are of minor importance [32]. However, they may play an important role for multivalent and macro-ions [33].

We assumed a permittivity of 78.5 for the surrounding water. Nevertheless, it is known that bound water has a reduced permittivity [34]. In addition, high ion concentrations will reduce the permittivity, especially in the vicinity of the charged surface. Taking these effects into account, e.g. by a position-dependent permittivity, will result in a minor correction of our calculations. It will lead to a slightly higher field close to the surface and reduce the condensation effect.

To improve the statistics of the system for cylinders, a length much greater than the radius has been assumed. While the number of lattice sites in a sphere decreases with radius in all possible directions, their number in the cylinder decreases only in the radial but not in the axis direction. Accordingly, in EVPB theory, the statistical double layer description inside nanotubes is not as restricted as in nanospheres.

This study has looked at the influence of ion size on the counterion concentration and the electrostatic potential near the inner surface of hollow cylindrical nanotubes filled with electrolyte solution. In conclusion, we have shown that for larger ions and larger surface charge densities, the effect of finite ion size is considerable and that strong discrepancies between the PB and EVPB theories may exist. The deviation from the predictions of the PB theory can be attributed to the steric effects in the EVPB approach. The PB theory predicted higher counterion concentrations close to the concave surface than the EVPB theory did, where the counterion concentration is limited to a plateau for large a. The plateau is reached when all available lattice sites of a layer have been filled.

Furthermore, we have examined the Tsao criterion for counterion condensation within the EVPB theory. We have been able to show that the concentration of counterions at the axis of the nanotube did not reach an upper limit at high surface charge density (Tsao condensation [27,28]) as predicted by the PB theory. Within EVPB theory, Tsao's condensation condition is not applicable in nanotubes. Alternatively, the close packing of large counterions near a highly charged surface, i.e. actual counterion condensation, predicted by EVPB theory can be observed directly.

Acknowledgements

We are grateful to R. Sleigh for help with the manuscript. A.I. has been supported by a fellowship for basic research from Deutscher Akademischer Austauschdienst funding his stay in Germany. The support of World Science Foundation (K.B.) and the Ministry of Science and Education of the Republic of Slovenia (K.B., V.K.I., T.S., A.I.) is acknowledged. This work has partly been supported by grant StSch 2002 0418A from Bundesamt für Strahlenschutz to J.G.

Appendix A. Minimization of the free energy

Assuming local thermodynamic equilibrium and taking into account energies of the individual particles in the solution, the expression for the free energy, the ion and solvent distribution functions and the differential equation for the electric potential are derived within the mean field approximation.

We divide the system into cells [8,35] of volume $\Delta V=2\pi rl\Delta r$ in cylindrical geometry and $\Delta V=4\pi r^2\Delta r$ in spherical geometry, where Δr is the dimension of the cell in the r direction. We assume that Δr is small compared to the distance over which macroscopic properties change essentially. In the cell we have N_j ions of the j-th species, $j=1, 2, \ldots, M$, and N_0 solvent molecules. The finite size of particles is introduced by means of the excluded volume effect. A lattice is introduced with all sites occupied: the particles are distributed over N_s^{cell} lattice sites of equal volume in the cell

$$\sum_{j=0}^{M} N_j = N_s^{cell}. \tag{A.1}$$

Any cell is open with respect to heat, and closed with respect to matter. The cell is characterized by the variables ΔV, temperature T, and the number of the particles of all species N_j, $j=0, 1, \ldots, M$, where $j=0$ corresponds to water molecules.

The free energy is obtained starting from the energy contributions of individual particles which are treated as independent and indistinguishable. The expression for the free energy of the solution in the cell can be obtained from the statistical mechanical relation $\Delta F=-kT\ln Q^{cell}$ [8,35,36],

$$\Delta F = \Delta W^{el} + kT\left(\sum_{j=0}^{M} n_j \ln \frac{n_j}{n_s q_j^0}\right)\Delta V \tag{A.2}$$

where Q^{cell} is the canonical partition function of the cell and ΔW^{el} is the electrostatic potential energy of the cell. The second term of the r.h.s. of Eq. (A.2) represents the entropic contribution to the free energy, q_j^0 is the non-electrostatic contribution to the partition function of a single particle of the j-th species subject to no electrostatic variable. The density of the number of particles of the j-th species n_j, $j=0, 1, \ldots, M$ and the density of the number of sites n_s were introduced

$$n_j = \frac{N_j}{\Delta V} \quad \text{and} \quad n_s = \frac{N_s^{cell}}{\Delta V}. \tag{A.3}$$

The Eq. (A.2) represents the free energy of the chosen cell. To obtain the free energy of the whole system, we sum the contributions of all cells, i.e. perform the integration

over the extension of the system in r. The electrostatic energy of the whole system is calculated by taking into account that the electrostatic potential at the site of a given ion is created by all other ions and the charged surface. The energy can be expressed using the equations of the classical theory of electromagnetism [8,35]:

$$W^{\mathrm{el}} = \frac{1}{2}\epsilon\epsilon_0 \int_0^{r_0} E^2(r) J(r) \mathrm{d}r \tag{A.4}$$

where $E(r)$ is the electric field strength and $J(r)$ is the Jacobian. In cylindrical geometry $J(r)=2\pi rl$, while in spherical geometry $J(r)=4\pi r^2$. Due to the cylindrical and spherical geometries the electrostatic field depends only on the radial coordinate.

The free energy of the whole system, subject to the local thermodynamic equilibrium, is

$$F = \int_0^{r_0} f(E(r), n(r)) J(r) \mathrm{d}r, \tag{A.5}$$

where the density of the free energy is given by

$$f(E(r), n(r)) = \frac{1}{2}\epsilon\epsilon_0 E^2(r) + kT\left(\sum_{j=0}^{M} n_j(r) \ln \frac{n_j(r)}{n_{\mathrm{s}} q_j^0}\right), \tag{A.6}$$

and $n(r)=(n_0, n_1, \ldots, n_M)$ is the density of the number of particles.

The particle distribution functions $n_j, j=0, 1, \ldots, M$ and the electric field strength are not known in advance. Thus, in the following, explicit expressions for functions $n_j(x), j=0, 1, \ldots, M$ and $E(r)$ are obtained using the condition of the free energy to be at its minimum at thermodynamic equilibrium of the whole system. The condition for the global equilibrium

$$\delta F = 0, \tag{A.7}$$

is subject to

- the global constraint requiring that the total number of particles of each species per volume of the whole system, Λ_j; is constant

$$\int_0^{r_0} \left(n_j(r) - \Lambda_j\right) J(r) \mathrm{d}r = 0, \quad j = 0, 1, 2, \ldots, M, \tag{A.8}$$

- the local constraint requiring the validity of the differential form of Gauss's law $\epsilon\epsilon_0 \nabla E = \varrho(r)$, where $\varrho(r) = e_0 \sum_{j=1}^{M} v_j n_j(r)$ is the volume charge density,

$$\epsilon\epsilon_0 \frac{1}{r^{\eta}} \frac{\partial (r^{\eta} E(r))}{\partial r} - e_0 \sum_{j=1}^{M} v_j n_j(r) = 0, \tag{A.9}$$

in the spherical geometry $\eta=2$ while in the cylindrical geometry $\eta=1$,

- and the local constraint requiring that all lattice sites are occupied

$$n_{\mathrm{s}} = \sum_{j=0}^{M} n_j(r). \tag{A.10}$$

The method of undetermined multipliers [37] has been used to find the extreme of the free energy Eq. (A.5) taking into account the constraints (Eqs. A.8 A.9 A.10). The variational problem can be expressed by Euler equations

$$\frac{\partial L^*}{\partial E} - \frac{\mathrm{d}}{\mathrm{d}r}\left(\frac{\partial L^*}{\partial \left(\frac{\partial E}{\partial r}\right)}\right) = 0, \tag{A.11}$$

$$\frac{\partial L^*}{\partial n_j} = 0, \quad j = 0, 1, 2, \ldots, M, \tag{A.12}$$

where

$$\begin{aligned} L^*&\left(E(r), n(r), \frac{\partial E(r)}{\partial r}, \tilde{\eta}_1(r), \tilde{\eta}_2(r)\right) \\ &= f(E(r), n(r)) J(r) + \sum_{j=0}^{M} \lambda_j \left(n_j(\mathrm{r}) - \Lambda_j\right) J(r) \\ &\quad - \tilde{\eta}_1(r)\left(\epsilon\epsilon_0 \frac{1}{r^{\eta}} \frac{\partial (r^{\eta} E(r))}{\partial r} - e_0 \sum_{j=1}^{M} v_j n_j(r)\right) \\ &\quad + \tilde{\eta}_2(r)\left(n_{\mathrm{s}} - \sum_{j=0}^{M} n_j(r)\right), \end{aligned} \tag{A.13}$$

λ_j, $j=0, 1, \ldots, M$, are the global Lagrange multipliers while $\tilde{\eta}_1$ and $\tilde{\eta}_2$ are the local Lagrange parameters. In the following the local Lagrange multipliers are expressed as

$$\tilde{\eta}_1(r) = \eta_1(r) J(r), \ \tilde{\eta}_2(r) = \eta_2(r) J(r). \tag{A.14}$$

Upon insertion of Eq. (A.14) into Eq. (A.13) we obtain

$$\begin{aligned} L^*&\left(E(r), n(r), \frac{\partial E(r)}{\partial r}, \eta_1(r), \eta_2(r)\right) / J(r) \\ &= f(E(r), n(r)) + \sum_{j=0}^{M} \lambda_j \left(n_j(r) - \Lambda_j\right) \\ &\quad - \eta_1(r)\left(\epsilon\epsilon_0 \frac{1}{r^{\eta}} \frac{\partial (r^{\eta} E(r))}{\partial r} - e_0 \sum_{j=1}^{M} v_j n_j(r)\right) \\ &\quad + \eta_2(r)\left(n_{\mathrm{s}} - \sum_{j=0}^{M} n_j(r)\right), \end{aligned} \tag{A.15}$$

At $r=0$ the electrostatic field vanishes

$$\left.\frac{\mathrm{d}\Phi}{\mathrm{d}r}\right|_{r=0} = 0, \tag{A.16}$$

meaning that the electrostatic potential at $r=0$ is constant,

$$\Phi|_{r=0} = \Phi_{\mathrm{c}}. \tag{A.17}$$

Eqs. (A.11, A.12) determine the local Lagrange multipliers

$$\eta_1(r) = \Phi(r), \tag{A.18}$$

$$\eta_2(r) = kT\left(\ln\frac{n_j}{n_s q_j^0} + 1 + \frac{\lambda_j}{kT}\right) + e_0 v_j \Phi(r). \tag{A.19}$$

From Eqs. (A.18, A.19) and the condition (Eq. A.17) the particle distribution functions (Eq. (4)) are obtained. The Gauss's law (Eq. A.9) and the particle distribution functions (Eq. (4)) give the differential equation for the electrostatic potential $\Phi(r)$ (Eq. (3)).

References

[1] V. Kralj-Iglič, M. Remškar, A. Iglič, in: A. Reimer (Ed.), Horizons in World Physics, Nova Science Publishers, Inc., New York, 2004, pp. 111–156.

[2] A. Karlsson, R. Karlsson, M. Karlsson, A.S. Cans, A. Strömberg, F. Ryttsen, O. Orwar, Networks of nanotubes and containers, Nature 409 (2001) 150–152.

[3] V. Kralj-Iglič, A. Iglič, G. Gomišček, F. Sevšek, V. Arrigler, H. Hägerstrand, Microtubes and nanotubes of a phospholipid bilayer membrane, J. Phys. A, Math. Gen. 35 (2002) 1533–1549.

[4] A. Rustom, R. Saffrich, I. Marković, P. Walther, H.H. Gerdes, Nanotubular highways for intercellular organelle transport, Science 303 (2004) 1007–1010.

[5] J.N. Israelachvili, Intermolecular and Surface Force, Academic Press Limited, 1992.

[6] S. McLaughlin, The electrostatic properties of membranes, Ann. Rev. Biophys. Biophys. Chem. 18 (1989) 113–136.

[7] A. Safran, Statistical Thermodynamics of Surfaces, Interfaces, and Membranes, Addison-Wesley Publishing Company, 1994.

[8] V. Kralj-Iglič, A. Iglič, A simple statistical mechanical approach to the free energy of the electric double layer including the excluded volume effect, J. Phys., II France 6 (1996) 477–491.

[9] I. Borukhov, D. Andelman, H. Orland, Steric effects in electrolytes: a modified Poisson Boltzmann equation, Phys. Rev. Lett. 79 (1997) 435–438.

[10] M. Manciu, E. Ruckenstein, Lattice site exclusion effect on the double layer interaction, Langmuir 18 (2002) 5178–5185.

[11] I. Borukhov, Charge renormalization of cylinders and spheres: ion size effect, J. Pol. Sci. B, Pol. Phys. 42 (2004) 3598–3615.

[12] F. Akoum, O. Parodi, Electrostatic interactions inside the aqueous core of spherical reversed micelles (L_2 phase), J. Phys. 46 (1985) 1675–1681.

[13] D. Bratko, A. Luzar, S.H. Chen, Electrostatic model for protein/reverse micelle complexation, J. Chem. Phys. 89 (1988) 545–550.

[14] N. Imai, T. Onishi, Analytical solution of Poisson–Boltzmann equation for two-dimensional many-center problem, J. Chem. Phys. 30 (1959) 1115–1116.

[15] F. Oosawa, Polyelectrolytes, Marcel Dekker, New York, 1970.

[16] V. Freise, Zur Theorie der diffusen Doppelschicht, Z. Elektrochem. 56 (1952) 822–827.

[17] M. Eigen, E. Wicke, The thermodynamics of electrolytes at higher concentrations, J. Phys. Chem. 58 (1954) 702–714.

[18] E. Trizac, J.L. Raimbault, Long-range electrostatic interactions between like-charged colloids: steric and confinement effects, Phys. Rev., E Stat. Phys. Plasmas Fluids Relat. Interdiscip. Topics 60 (1999) 6530–6533.

[19] G. Barbero, L.R. Evangelista, D. Olivero, Asymmetric ionic adsorption and cell polarization in liquid crystals, J. Appl. Phys. 87 (2000) 2646–2648.

[20] L. Lue, N. Zoeller, D. Blankschtein, Incorporation of nonelectrostatic interactions in the Poisson–Boltzmann equation, Langmuir 15 (1999) 3726–3730.

[21] C.W. Outhwaite, S. Lamperski, A treatment of the exclusion volume term in the inhomogeneous Poisson–Boltzmann theory for ion–dipole mixture, Condens. Matter Phys. 4 (2001) 739.

[22] S.L. Carnie, G.M. Torrie, The statistical mechanics of the electrical double layer, Adv. Chem. Phys. 56 (1984) 141–253.

[23] L.B. Bhuiyan, C.W. Outhwaite, D. Bratko, Structure and thermodynamics of micellar solutions in the modified Poisson–Boltzmann theory, Chem. Phys. Lett. 193 (1992) 203–210.

[24] D. Bratko, Hypernetted chain approximation for ion distribution in reverse micelles, Chem. Phys. Lett. 169 (1990) 555–560.

[25] E. Gonzales-Tovar, M. Lozada-Cassou, D. Henderson, Hypernetted chain approximation for the distribution of ions around a cylindrical electrode: II. Numerical solution for a model cylindrical polyelectrolytes, J. Chem. Phys. 83 (1985) 361–372.

[26] K. Bohinc, V. Kralj-Iglič, A. Iglič, Thickness of electrical double layer. Effect of ion size, Electrochim. Acta 46 (2001) 3033–3040.

[27] H.-K. Tsao, Counterion distribution enclosed in a cylinder and a sphere, J. Phys. Chem., B 102 (1998) 10243–10247.

[28] H.-K. Tsao, Effects of salt addition on the ion distribution enclosed in a cylinder and a sphere, Langmuir 15 (1999) 4981–4988.

[29] N. Cuvillier, F. Rondelez, Breakdown of the Poisson–Boltzmann description for electrical double layers involving large multivalent ions, Thin Solid Films 327–329 (1998) 19–23.

[30] V. Kralj-Iglič, A. Iglič, H. Hägerstrand, P. Peterlin, Stable tubular microexovesicles of the erythrocyte membrane induced by dimeric amphiphiles, Phys. Rev. 61 (2000) 4230–4234.

[31] R.W. Baker, Membrane Technology and Applications, John Wiley & Sons, Ltd, 2004.

[32] V. Vlachy, Ionic effects beyond Poisson–Boltzmann theory, Annu. Rev. Phys. Chem. 50 (1999) 145–165.

[33] K.S. Schmitz, Macroions in Solution and Colloidal Suspension, VCH Publishers, New York, 1993.

[34] G. Cevc, Membrane electrostatics, Biochimica et Biophysica Acta 1031–3 (1990) 311–382.

[35] K. Bohinc, V. Kralj-Iglic, A. Iglič, T. Slivnik, Charged cylindrical surfaces: effect of finite ion size, Bioelectrochemistry 57 (2002) 73–81.

[36] T.L. Hill, An Introduction to Statistical Thermodynamics, Addison Wesley Publishing Company Inc., Reading, 1962.

[37] L.E. Elsgolc, Calculus of Variations, Pergamon Press, Oxford, 1961.